Thermodynamic insights into an interaction between ACYL-CoA–BINDING PROTEIN2 and LYSOPHOSPHOLIPASE2 in *Arabidopsis*

Received for publication, November 27, 2018, and in revised form, February 12, 2019 Published, Papers in Press, February 19, 2019, DOI 10.1074/jbc.RA118.006876

Rui Miao[‡], **Shiu-Cheung Lung**[‡], **Xin Li**[§], **Xiang David Li**[§], **and Mee-Len Chye**[‡¶1]

From the [‡]*School of Biological Sciences and* [§]*Department of Chemistry, University of Hong Kong, Pokfulam Road, Hong Kong and the* [¶]*State Key Laboratory of Agrobiotechnology, Chinese University of Hong Kong, Shatin N.T., Hong Kong, China*

Edited by Joseph M. Jez

Lysophospholipids (LPLs) are important lipid-signaling molecules in plants, of which lysophosphatidylcholine (lysoPC) is one of the most well-characterized LPLs, having important roles in plant stress responses. It is broken down by lysophospholipases, but the molecular mechanism involved in lysoPC degradation is unclear. Recombinant *Arabidopsis thaliana* ACYL-CoA–BINDING PROTEIN2 (AtACBP2) has been reported to bind lysoPC via its acyl-CoA–binding domain and also LYSOPHOSPHOLIPASE 2 (AtLYSOPL2) via its ankyrin repeats *in vitro*. To investigate the interactions of AtACBP2 with AtLYSOPL2 and lysoPC in more detail, we conducted isothermal titration calorimetry with $AtACBP2_{70-354}$, an AtACBP2 derivative consisting of amino acids 70–354, containing both the acyl-CoA–binding domain and ankyrin repeats. We observed that the interactions of $AtACBP2_{70-354}$ with AtLYSOPL2 and lysoPC were both endothermic, favored by solvation entropy and opposed by enthalpy, with dissociation constants in the micromolar range. Of note, three AtLYSOPL2 catalytic triad mutant proteins (S147A, D268A, and H298A) bound lysoPC only weakly, with an exothermic burst and dissociation constants in the millimolar range. Furthermore, the binding affinity of lysoPC-premixed $AtACBP2_{70-354}$ to AtLYSOPL2 was 10-fold higher than that of $AtACBP2_{70-354}$ alone to AtLYSOPL2. We conclude that AtACBP2 may play a role in facilitating a direct interaction between AtLYSOPL2 and lysoPC. Our results suggest that $AtACBP2_{70-354}$ probably binds to lysoPC through a hydrophobic interface that enhances a hydrotropic interaction of $AtACBP2_{70-354}$ with AtLYSOPL2 and thereby facilitates AtLYSOPL2's lysophospholipase function.

Phospholipids are crucial components of many biological membranes (1). Lysophospholipids (LPLs)[2] and free fatty acids are produced through the removal of an *O*-acyl chain (*sn*-1/*sn*-2) from phospholipids by phospholipase hydrolysis (2). LPLs are believed to be critical lipid-signaling molecules in cellular membranes (3). Plant LPLs normally exist in low amounts but can be elevated by environmental stimuli, such as low temperature and pathogen stress (4, 5). One of the most well-characterized LPLs is lysophosphatidylcholine (lysoPC) (6, 7). LysoPC has been reported to enhance pathogen susceptibility in tobacco plants via signaling pathways associated with the accumulation of reactive oxygen species and ethylene (8). As membrane-derived signaling molecules in eukaryotes, LPLs perform various biological functions through activating distinct signal transduction pathways (6, 9). LysoPC activates human T lymphocytes (10), up-regulates the expression of P-selectin in mammalian platelets and endothelial cells (11), and promotes nerve growth factor–induced signals in rat pheochromocytoma PC12 cells and neurotrophin-like activity in cerebellar granule neurons and PC12 cells (12). In mammalian cells, LPL signaling is supported by G protein–coupled plasma membrane receptors (13–15).

Lysophospholipases belong to a family of hydrolases that hydrolyze lysoPC by cleaving its carboxylic ester bond (16). In this enzymatic reaction, lysoPC and water are the substrates, and glycerophosphocholine and free fatty acid are the products (17). Based on sequence alignments, two classes of lysophospholipases have emerged in *Arabidopsis thaliana*, including LYSOPHOSPHOLIPASE1 (AtLYSOPL1; AT2G39400) and five AtLYSOPL1-like proteins (AT2G39400, AT2G39410, AT2G39420, AT3G55180, and AT3G55190), and LYSOPHOSPHOLIPASE2 (AtLYSOPL2; AT1G52760) (18). AtLYSOPL1, which functions in plant defense, was reported to be pathogen- and salicylic acid–inducible, but few studies have been conducted on the others (18, 19). AtLYSOPL2 can be grouped with monoacylglycerol lipases (MAGL), including 15 *Arabidopsis* homologues of the AtLYSOPL1 family, because they all showed high sequence homology in BLAST scores (≥75) to human monoglyceride lipase (MGL) (GB NP_009214), and all 16 *Arabidopsis* putative MAGLs (AtMAGLs) displayed 3D structures that are similar to a *Homo sapiens* MAGL (HsMAGL) (Protein Data Bank code 3HJU) (20, 21). In

This work was supported by the Wilson and Amelia Wong Endowment Fund, Research Grants Council of the Hong Kong Special Administrative Region, China, Grants 17101818, AoE/M-05/12, and AoE/M-403/16, and Innovation Technology Fund of the Innovation Technology Commission (Funding Support to State Key Laboratory of Agrobiotechnology in Hong Kong). The authors declare that they have no conflicts of interest with the contents of this article.

This article contains Figs. S1–S7 and Table S1.

[1] To whom correspondence should be addressed: School of Biological Sciences, University of Hong Kong, Pokfulam Rd., Hong Kong SAR, China. Tel.: 852-2299-0319; E-mail: mlchye@hku.hk.

[2] The abbreviations used are: LPL, lysophospholipid; lysoPC, lysophosphatidylcholine; ITC, isothermal titration calorimetry; aa, amino acid; ROS, reactive oxygen species; MAGL, monoacylglycerol lipase; MGL, monoglyceride lipase; ACBP, acyl-CoA–binding protein; ABA, abscisic acid; RCAR, regulatory component of ABA receptor.

addition, AtLYSOPL2 (AT1G52760) was also identified as a caffeoyl shikimate esterase, an enzyme central to the lignin biosynthetic pathway (22).

The interaction between AtLYSOPL2 and Acyl-CoA–binding Protein2 (AtACBP2; AT4G27780) was first demonstrated by yeast two-hybrid analysis and co-immunoprecipitation assays (19). Their subcellular interaction was verified by the co-localization of autofluorescence-tagged AtACBP2 and AtLYSOPL2 to the plasma membrane by confocal microscopy of agroinfiltrated tobacco leaves (19). Both proteins have been reported to independently function in conferring tolerance to cadmium (Cd) and oxidative stresses in transgenic *Arabidopsis* (19, 23).

Cd, highly toxic to plants, accumulates in food chains leading to adverse effects on human and animal health (24). Plants absorb Cd through their roots and accumulate it in shoots via zinc (Zn)/Cd-transporting ATPases (25, 26) and phytochelatin transporters (26, 27). Cd, "resembling common metal cofactors" such as Zn and calcium, inhibits protein function by binding to cysteine residues (28) and disrupts enzyme activity and signal transduction (29, 30). Cd accesses plant cells via calcium (Ca), iron (Fe), and Zn transporters/channels (24, 31) and causes deleterious effects via nitric oxide and reactive oxygen species (ROS) that can result in cell death (32). The roots of *Arabidopsis* mutants lacking SNF1-RELATED PROTEIN KINASE TYPE 2 displayed lower Cd-induced ROS accumulation, suggesting that these kinases regulate Cd-induced ROS (33). Transgenic *Arabidopsis* overexpressing AtLYSOPL2 and those overexpressing AtACBP2 were more tolerant to Cd than the WT (19). It has been suggested that AtLYSOPL2 overexpressors were more tolerant to H_2O_2 and Cd than the wildtype (WT) because AtLYSOPL2 enhances phospholipid repair following lipid peroxidation (19). Both *AtLYSOPL2* and *AtACBP2* mRNAs were elevated by Cd treatment; Zn and hydrogen peroxide (H_2O_2), but not lead (Pb), Cd, or copper (Cu), induced *AtLYSOPL2* expression in shoots, whereas only H_2O_2 up-regulated *AtLYSOPL2* expression in roots (19). Microarray data from the *Arabidopsis* Electronic Fluorescent Pictograph Browser revealed that *AtLYSOPL2* was inducible by biotic stresses caused by salicylic acid, bacterial-derived elicitor Flg22, and *Pseudomonas syringae*, besides various abiotic stresses, including cold, drought, genotoxicity (bleomycin plus mitomycin), oxidative treatment (methyl viologen), UV-B light, wounding, heat, and selenium (34). Western blot analysis using AtLYSOPL2 antibodies indicated that Cd and Zn treatments resulted in AtLYSOPL2 accumulation in shoots and roots, although Cd treatment down-regulated *AtLYSOPL2* expression in Northern blotting (19). Northern blotting analyses revealed a higher *AtLYSOPL2* expression in stems, flowers, and roots than in siliques and leaves (19).

To better understand the role of AtACBP2 and AtLYSOPL2 in stress tolerance, the *in vitro* energetics of their interactions were investigated. The thermodynamic analysis reported here provides new insights on AtACBP2, AtLYSOPL2, and lysoPC interactions.

Results

AtACBP2$_{70-354}$ binds both lysoPC (C16:0) and palmitoyl-CoA thioester

AtACBP2 (AT4G27780) consists of amino acids (aa) 1–354 comprising a signal peptide (aa 1–6), transmembrane domain (aa 7–69), the acyl-CoA–binding domain (aa 70–214) and the ankyrin repeats (aa 215–354) (Fig. 1*A*). The transmembrane domain (aa 7–69) was deleted in AtACBP2$_{70-354}$, because the truncated version (AtACBP2$_{70-354}$) enhanced AtACBP2 expression and solubility. The AtACBP2$_{70-354}$ interaction with lipid ligands and AtLYSOPL2 was assessed by isothermal titration calorimetry (ITC), which quantifies the binding equilibrium directly by measuring the heat change resulting from the association of a ligand with its binding partner (35). ITC thermograms showed that AtACBP2$_{70-354}$, an AtACBP2 derivative consisting of aa 70–354 inclusive of the acyl-CoA–binding domain and the ankyrin repeats, binds to both lysoPC (C16:0) and palmitoyl-CoA (C16:0–CoA) thioesters (Fig. 1, *B* and *C*). The primary heat change of AtACBP2$_{70-354}$–lysoPC (Fig. 1*B*) and AtACBP2$_{70-354}$–C16:0–CoA (Fig. 1*C*) interactions was fitted using a simple one-site binding model to yield the thermodynamic parameters (Table 1). AtACBP2$_{70-354}$ showed a higher binding affinity to C16:0–CoA than lysoPC, with K_D values of 0.64 and 39.2 μM, respectively (Table 1).

Interestingly, the thermodynamic characteristics of interactions between AtACBP2$_{70-354}$–lysoPC (Fig. 1*B*) and AtACBP2$_{70-354}$–C16:0–CoA (Fig. 1*C*) were fundamentally different. AtACBP2$_{70-354}$–lysoPC interaction represented an unusual endothermic association with favorable entropy ($-T\Delta S$ −22.17 kcal mol^{-1}) and opposed by enthalpy (ΔH 16.17 kcal mol^{-1}) (Table 1), which suggests that the binding of AtACBP2$_{70-354}$ to lysoPC is supported by hydrophobic interactions (Fig. 1*D*). For lysoPC, the stoichiometric value (n) was 1.22, indicating that one molecule of AtACBP2$_{70-354}$ binds to only one lysoPC ligand (Table 1).

The AtACBP2$_{70-354}$–C16:0–CoA interaction was exothermic, favored by both enthalpy (ΔH −4.51 kcal mol^{-1}) and entropy ($-T\Delta S$ −3.93 kcal mol^{-1}), suggesting that the binding of AtACBP2$_{70-354}$ to C16:0–CoA is composed of hydrogen bonding and hydrophobic interactions (Fig. 1*D*). In addition, the interaction between AtACBP2$_{70-354}$ and C16:0–CoA showed an n value of 1.73 (Table 1), indicating that one molecule of AtACBP2$_{70-354}$ likely binds to two C16:0–CoA ligands. The stoichiometry value observed here resembles that ($n = 1.7$) previously reported for the C2B and C2G domains of dysferlin, which was presumed to bind to two Ca^{2+} ions (36).

AtACBP2$_{70-354}$ binds to WT AtLYSOPL2 and the WT AtLYSOPL2–lysoPC complex

The effect of lysoPC on the AtLYSOPL2–AtACBP2$_{70-354}$ (Fig. 2*A*) interaction was determined by ITC. Theoretical fits to the experimental data were achieved using a single binding site model with the thermodynamic parameters listed in Table 2, including dissociation constant (K_D), stoichiometry of the ligand-to-protein binding (n), enthalpy change (ΔH), the entropy change (ΔS), and free energy change (ΔG). ITC thermograms revealed that binding of AtLYSOPL2 (Fig. 2*B*) or the

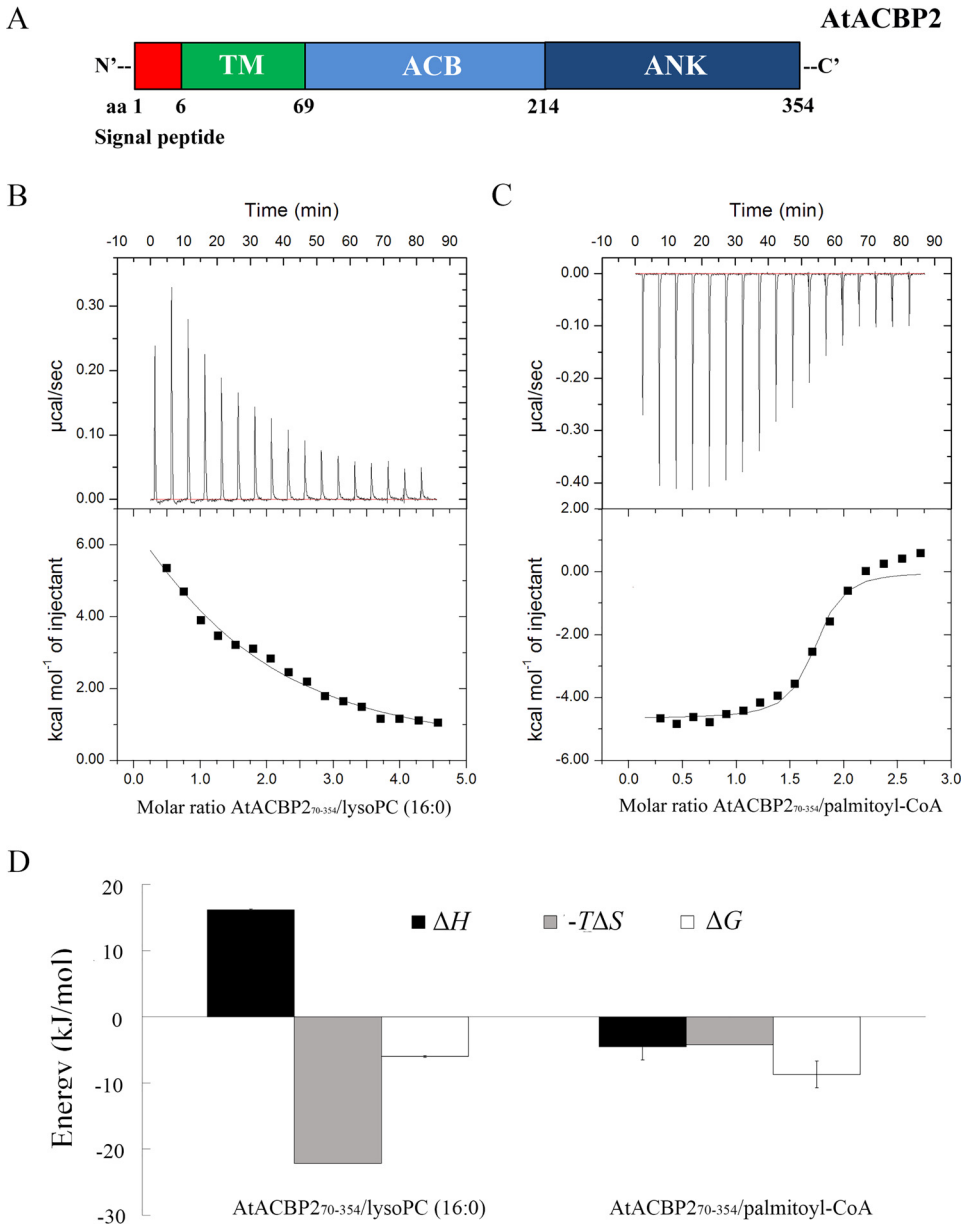

Figure 1. ITC analysis of AtACBP2$_{70-354}$ interactions with lysoPC (C16:0) and C16:0–CoA. *A,* schematic representation of the domains in *Arabidopsis* AtACBP2. The signal peptide (aa 1–6), transmembrane (TM) domain (aa 7–69), acyl-CoA binding (ACB) domain (aa 70 to 214), and ankyrin repeats (ANK) (aa 215–354) of AtACBP2 are shown in *red*, *green*, *light blue*, and *dark blue*, respectively. AtACBP2$_{70-354}$ consists of a derivative lacking the transmembrane domain, with the ACB and ANK domains intact. AtACBP2$_{215-354}$ consists of the ANK domain. *B,* AtACBP2$_{70-354}$ and lysoPC (C16:0) binding measured by titrating 30–40 μM AtACBP2$_{70-354}$ in the chamber with 600–800 μM lysoPC (C16:0) in the syringe. *C,* AtACBP2$_{70-354}$ and C16:0–CoA binding measured by titrating 30–40 μM AtACBP2$_{70-354}$ in the chamber with 600–800 μM C16:0–CoA in the syringe. *Top panel*, raw heating power over time; *bottom panel*, fit of the integrated energy values normalized for injected protein. *D,* binding signature (ΔH, $-T\Delta S$, and ΔG) plotted for AtACBP2$_{70-354}$–lysoPC (C16:0) and AtACBP2$_{70-354}$–C16:0–CoA interactions. Binding enthalpy, entropy, and free energy are shown in *black*, *gray*, and *white*, respectively. The values originate from Table 1. *Error bars* denote S.E., $n = 2$.

Table 1

ITC binding constants and thermodynamic parameters for AtACBP2$_{70-354}$ interactions with palmitoyl-CoA and lysoPC

The values are plotted in Fig. 1. Experiments were carried out at 25 °C, and each value is the mean of at least two independent titrations. *n* is number of binding sites (n = ligand/receptor); K_D is dissociation constant; ΔH is enthalpy change; ΔS is entropy change; ΔG, Gibbs free energy. The binding entropy and enthalpy determine ligand binding. Positive is unfavorable, and negative is favorable (61, 62).

Combinations	*n*	K_D	ΔH	$-T\Delta S$	ΔG
		μM	kcal mol^{-1}	kcal mol^{-1}	kcal mol^{-1}
AtACBP2$_{70-354}$/palmitoyl-CoA	1.73 ± 0.03	0.64 ± 0.09	−4.51 ± 0.13	−3.93	−8.44 ± 0.13
AtACBP2$_{70-354}$/lysoPC	1.22 ± 0.42	39.2 ± 8.4	16.17 ± 6.8	−22.17	−6.05 ± 6.8

AtLYSOPL2–lysoPC complex (Fig. 2*C*) to AtACBP2$_{70-354}$ was highly endothermic. The interactions were driven by favorable entropy $-T\Delta S$ of −15.38 and −15.29 kcal mol^{-1} and opposed by enthalpy changes ΔH of 9.55 and 9.65 kcal mol^{-1}, respectively (Table 2). The binding mechanism of AtLYSOPL2–AtACBP2$_{70-354}$ is similar to AtACBP2$_{70-354}$–lysoPC and is

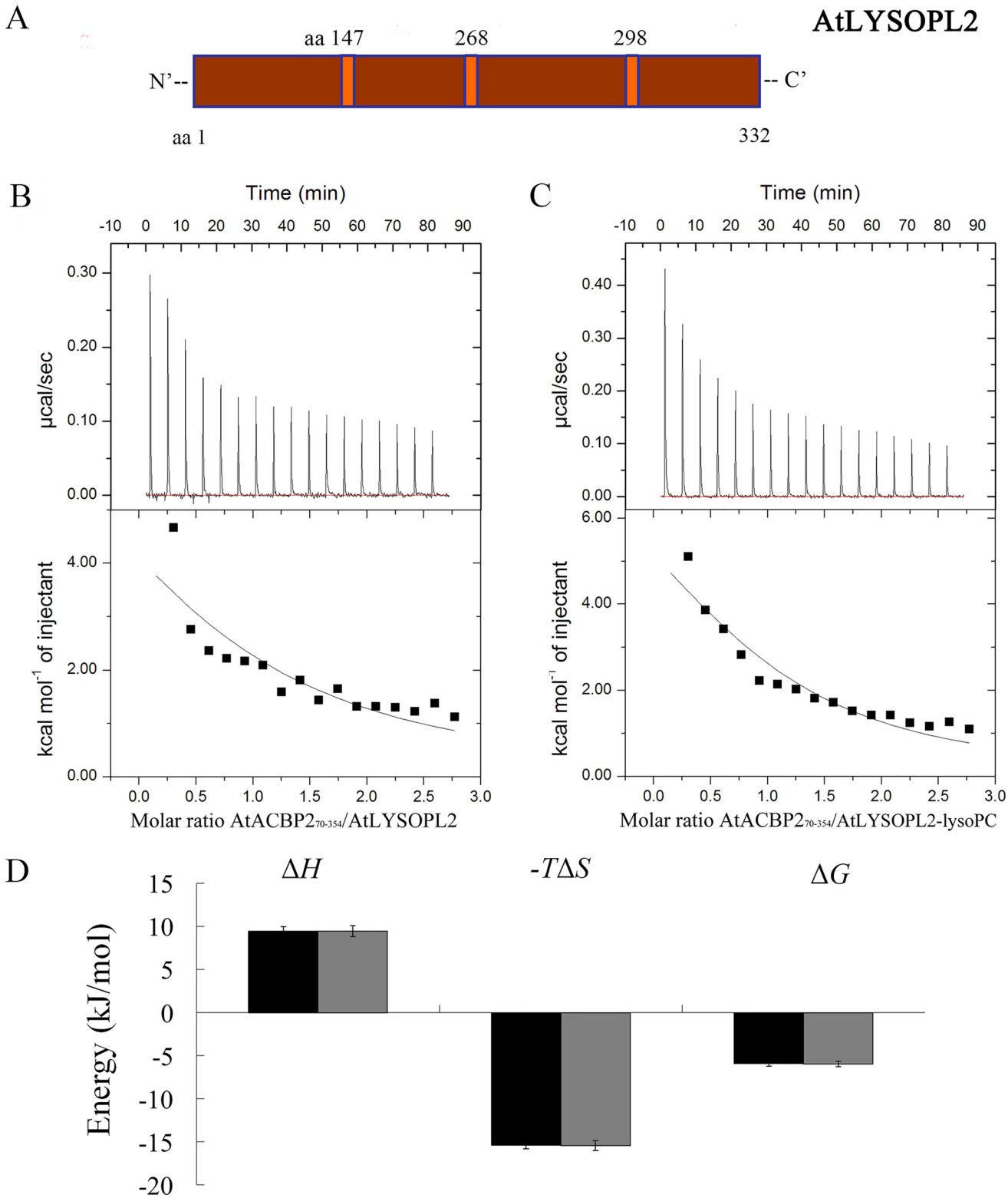

Figure 2. ITC analysis of AtLYSOPL2, AtACBP2$_{70-354}$, and lysoPC interactions. *A,* schematic representation of the structure of *Arabidopsis* AtLYSOPL2. The catalytic triad of AtLYSOPL2 is shown in *orange*. *B,* interactions between AtLYSOPL2 and AtACBP2$_{70-354}$. Binding was tested in ITC by titrating 30–40 μM AtLYSOPL2 in the chamber with 400–500 μM AtACBP2$_{70-354}$ in the syringe. *C,* interactions between the AtLYSOPL2–lysoPC (molar ratio 1:1) complex and AtACBP2$_{70-354}$. Binding was tested in ITC by titrating 30 μM AtLYSOPL2–lysoPC complex in the chamber with 400–500 μM AtACBP2$_{70-354}$ in the syringe. *Top panel*, raw heating power over time; *bottom panel*, fit of the integrated energy values normalized for injected protein. *D,* energetics of AtLYSOPL2 interaction with AtACBP2$_{70-354}$. Plots of the binding signature (ΔH, $-T\Delta S$, and ΔG) with interactions of AtLYSOPL2 and AtACBP2$_{70-354}$ in the absence of lysoPC shown in *black*, and AtLYSOPL2 and AtACBP2$_{70-354}$ in the presence of lysoPC in *gray*. The values were obtained from data presented in Table 2. *Error bars* denote S.E., $n = 3$. The values originate from Table 2.

Table 2

ITC binding constants and thermodynamic parameters for interactions of AtLYSOPL2 wildtype or mutant proteins with AtACBP2$_{70-354}$ with/without lysoPC

The values are plotted in Figs. 2 and 5. Experiments were carried out at 25 °C, and each value is the mean of three independent titrations. n is number of binding sites (n = ligand/receptor); K_D is dissociation constant; ΔH is enthalpy change; ΔS is entropy change; ΔG is Gibbs free energy. The binding entropy and enthalpy determine ligand binding. Positive is unfavorable, and negative is favorable (61, 62).

Combinations	n	K_D	ΔH	$-T\Delta S$	ΔG
		μM	kcal mol^{-1}	kcal mol^{-1}	kcal mol^{-1}
AtACBP2$_{70-354}$/wildtype AtLYSOPL2	1.05 ± 0.01	28.98 ± 3.36	9.55 ± 0.26	−15.38 ± 0.13	−5.93 ± 0.12
AtACBP2$_{70-354}$/wildtype AtLYSOPL2-lysoPC	1.17 ± 0.5	29.99 ± 3.86	9.65 ± 4	−15.29 ± 3.87	−5.63 ± 2.87
AtACBP2$_{70-354}$/AtLYSOPL2 S147A	0.56 ± 0.2	20.7 ± 1.03	10.71 ± 3.19	−15.7 ± 3.21	−4.99 ± 2.2
AtACBP2$_{70-354}$/AtLYSOPL2 S147A-lysoPC	0.36 ± 0.09	15.02 ± 1.63	18.1 ± 2.17	−24.47 ± 1.77	−6.37 ± 1.9
AtACBP2$_{70-354}$/AtLYSOPL2 D268A	0.37 ± 0.08	12.39 ± 0.24	9.27 ± 1.16	−15.94 ± 1.18	−6.67 ± 1.4
AtACBP2$_{70-354}$/AtLYSOPL2 D268A-lysoPC	0.31 ± 0.12	10.17 ± 4.32	9.63 ± 2.46	−16.42 ± 1.79	−6.79 ± 1.88
AtACBP2$_{70-354}$/AtLYSOPL2 H298A	0.84 ± 0.03	25.64 ± 2.49	6.42 ± 1.2	−12.67 ± 1.45	−5.27 ± 1.84
AtACBP2$_{70-354}$/AtLYSOPL2 H298A-lysoPC	0.67 ± 0.66	23.04 ± 2.14	7.63 ± 0.7	−14.23 ± 1.12	−6.62 ± 1.11

assumed to be based on hydrophobic interactions following a conformational change (Fig. 2*D*).

The K_D value for the AtLYSOPL2 and AtACBP2$_{70-354}$ interaction was 28.98 μM (Table 2). A similar affinity as reflected by a K_D value of 29.99 μM when AtACBP2$_{70-354}$ was titrated to the preformed AtLYSOPL2–lysoPC complex (molar ratio 1:1) demonstrating that lysoPC, when pre-bound to AtLYSOPL2, did not promote the AtLYSOPL2 and AtACBP2$_{70-354}$ interaction (Table 2). Only one binding site was predicted for the AtLYSOPL2 and AtACBP2$_{70-354}$ interaction, because ITC data showed an n value of 1.05 (Table 2).

Role of the conserved catalytic triad in AtLYSOPL2

Structural sequence alignments of AtLYSOPL2, AtLYSOPL1, and human MGL were analyzed using the Jalview version 1.6 software (http://www.jalview.org/)[3] (Fig. S1) (63). The Fig. S1 identified three conserved catalytic residues (Ser-147, Asp-268, and His-298) in AtLYSOPL2, corresponding to the catalytic triad (Ser-132, Asp-249, and His-279) of MGL (21). AtLYSOPL2 showed 28% aa sequence homology to MGL and 34% homology to AtLYSOPL1, whereas AtLYSOPL1 showed 31% homology to MGL. Phylogenetic analysis indicated that AtLYSOPL2 stands by itself and displayed low aa sequence identities with other homologues in *A. thaliana* (Fig. S2).

To construct a 3D structural model for AtLYSOPL2, the X-ray crystal structure of human MGL, an orthologue of AtLYSOPL2, was used as a structural template for analysis with the MODELLER program (Fig. 3*A*). When the positions for lysoPC binding were predicted using the AutoDock program (http://autodock.scripps.edu/),[3] lysoPC (C16:0) was found to lie in a pocket-like binding site on AtLYSOPL2 (Fig. 3, *B* and *C*). The conserved AtLYSOPL2 catalytic triad, Ser-147, Asp-268, and His-298, was observed located adjacent to lysoPC, suggesting its potential significance in an enzymatic reaction (Fig. 3*D*).

To validate these docking analyses, single point mutations (*i.e.* S147A, D268A, and H298A) were generated by site-directed mutagenesis and proteins purified (Fig. S3). Results from GC-MS analysis, using lysoPC (C16:0) as a substrate in enzymatic assays, demonstrated that hexadecanoic acid was produced, verifying AtLYSOPL2 function as a typical lysophospholipase *in vitro*. In contrast, AtLYSOPL2 mutant proteins S147A, D268A, and H298A lack lysophospholipase activity,

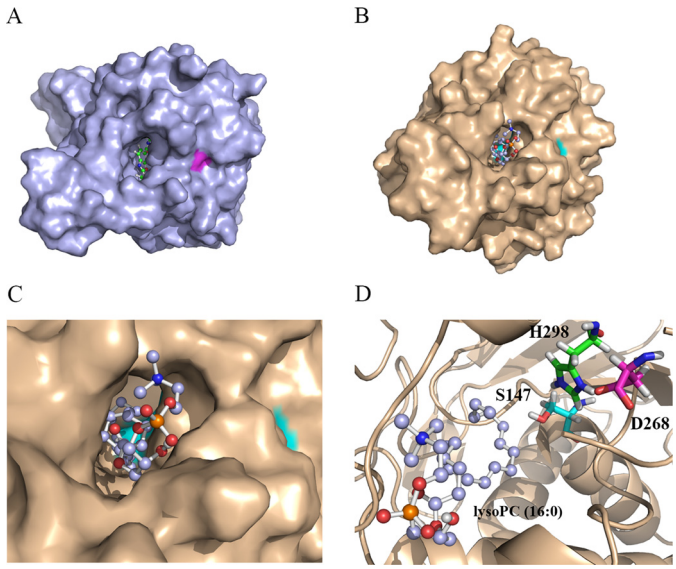

Figure 3. Homology modeling and dock simulation of lysoPC (C16:0) binding to AtLYSOPL2. *A,* structure of human MGL with its inhibitor JZL184 (Protein Data Bank code 3JWE (21). *B* and *C,* 3D structure model of AtLYSOPL2 with lysoPC (C16:0). The bottom catalytic residues in the pocket-like cleavage site are shown in *cyan*. *D,* putative scissor aa residues Ser-147, Asp-268, and His-298 in the cleavage site of AtLYSOPL2. LysoPC (C16:0) is shown as *ball* and *stick*.

and little to no hexadecanoic acid was produced (Fig. 4, *A* and *B*). The relative lysophospholipase activities of the AtLYSOPL2 mutant proteins S147A, D268A, and H298A were 0.10, 0.08, and 0.12, respectively, and compared with the WT AtLYSOPL2 protein value of 1 (Fig. 4*A*), indicating that all three conserved catalytic aa residues are essential for lysophospholipase catalysis.

AtACBP2$_{70-354}$ binds to AtLYSOPL2 catalytic triad mutant proteins and the AtLYSOPL2 catalytic triad mutant—lysoPC complexes

To analyze whether the AtLYSOPL2 catalytic triad influences the interaction between AtLYSOPL2 and AtACBP2, ITC experiments were performed using AtLYSOPL2 WT and mutant (S147A, D268A, and H298A) proteins in the presence and absence of lysoPC and AtACBP2$_{70-354}$. The ITC results were again fitted using a single binding site model. Thermodynamic properties of interactions between WT and mutant AtLYSOPL2 to AtACBP2$_{70-354}$ were similar. All appeared to be endothermic, and the interactions were favored by a change of

[3] Please note that the JBC is not responsible for the long-term archiving and maintenance of this site or any other third party hosted site.

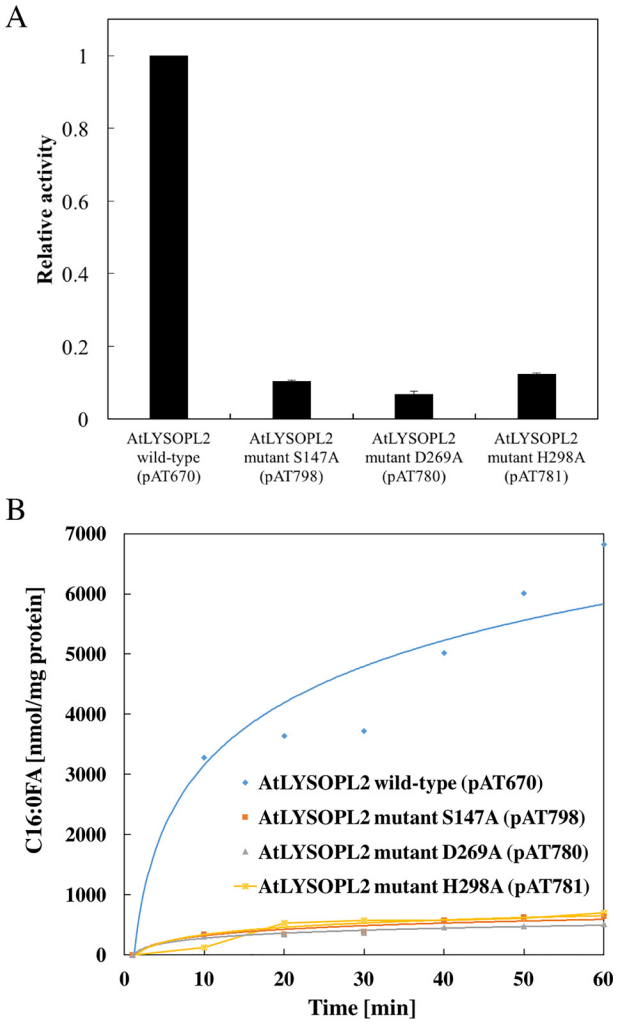

Figure 4. Lysophospholipase activity assays on AtLYSOPL2 and its mutant derivatives. *A,* comparison of lysophospholipase activity among WT AtLYSOPL2 and its mutant proteins (S147A, D268A, and H298A). The values are shown as the relative activity to WT AtLYSOPL2 (defined value of 1). *B,* amount of C16:0-FA detected at different time intervals.

entropy ($-T\Delta S$), but opposed by an unfavorable enthalpy (ΔH) change (Fig. 5 and Table 2).

The binding affinities of S147A, D268A, and H298A to AtACBP2$_{70-354}$ were similar to WT AtLYSOPL2 and AtACBP2$_{70-354}$ (K_D = 28.98 μM). In the absence of lysoPC, interactions between AtACBP2$_{70-354}$ and S147A, D268A, or H298A yielded K_D values of 20.7, 12.39, and 25.64 μM, respectively (Fig. 5, *A–C*, and Table 2), which were similar to interactions between AtACBP2$_{70-354}$ and S147A, D268A, and H298A in the presence of lysoPC (K_D = 15.02, 10.17, and 23.04 μM, respectively) (Fig. 5, *D–F*, and Table 2). These results demonstrated that the presence of lysoPC did not enhance interactions between AtACBP2$_{70-354}$ and S147A, D268A, and H298A, when premixed with the mutant protein at a 1:1 molar ratio.

Binding of WT AtLYSOPL2 or AtLYSOPL2 catalytic triad mutant proteins to AtACBP2$_{70-354}$–lysoPC complex

To identify the effect of the preformed AtACBP2$_{70-354}$–lysoPC complex (molar ratio 1:1) on interaction with WT AtLYSOPL2 or AtLYSOPL2 catalytic triad mutant proteins (S147A, D268A, and H298A), thermodynamic parameters were again determined by ITC and fitted through a simple one-site binding model. The AtACBP2$_{70-354}$–lysoPC (molar ratio 1:1) complex was titrated to the WT AtLYSOPL2 or AtLYSOPL2 mutant proteins (S147A, D268A, and H298A). The results revealed that the interactions of the AtACBP2$_{70-354}$–lysoPC complex with WT AtLYSOPL2 and AtLYSOPL2 catalytic triad mutant proteins were endothermic, favored entirely by entropy ($-T\Delta S$) and opposed by enthalpy (ΔH) (Fig. 6*A* and Table 3). However, the dissociation constant (K_D = 1.69 μM) (Table 3) declined 12-fold compared with AtACBP2$_{70-354}$ binding to AtLYSOPL2 S147A (K_D = 20.7 μM) (Table 3).

The binding affinities of AtLYSOPL2 mutant proteins (S147A, D268A, and H298A) to AtACBP2$_{70-354}$ were similar to that of WT AtLYSOPL2 with AtACBP2$_{70-354}$ (K_D = 28.98 μM). In the absence of lysoPC, the interactions between AtACBP2$_{70-354}$ and AtLYSOPL2 mutant proteins (S147A, D268A, and H298A) yielded K_D values of 20.7, 12.39, and 25.64 μM, respectively (Table 3). However, the dissociation constant declined in interactions between the AtACBP2$_{70-354}$–lysoPC complex and AtLYSOPL2 mutant proteins (S147A, D268A, and H298A), which had K_D values of 1.69, 1.38, and 0.89 μM, respectively (Table 3). These data demonstrated that lysoPC enhanced the interactions between AtACBP$_{70-354}$ and AtLYSOPL2 mutant proteins (S147A, D268A, and H298A) when it was premixed with AtACBP2$_{70-354}$ at a 1:1 molar ratio.

To address whether the ankyrin repeats or the acyl-CoA–binding domain of AtACBP2 influences its interaction with AtLYSOPL2, ITC experiments were performed by titrating AtACBP2$_{70-214}$ (lacking the ankyrin repeats) or AtACBP2$_{215-354}$ (lacking the acyl-CoA–binding domain), in the presence or absence of lysoPC, into WT AtLYSOPL2 or AtLYSOPL2 catalytic triad mutant (S147A, D268A, and H298A) proteins. No interaction was detected in all combinations involving AtACBP2$_{70-214}$ or AtACBP2$_{215-354}$ (Fig. S4 and Table 3). This demonstrated that the presence of both the ankyrin repeats and the acyl-CoA–binding domain of AtACBP2 was crucial for its binding to AtLYSOPL2.

Binding of WT AtLYSOPL2 or AtLYSOPL2 catalytic triad mutant proteins to lysoPC

Arising from its lysophospholipase activity (Fig. 4), WT AtLYSOPL2 could not be used in ITC experiments to determine the thermodynamic parameters for its binding to lysoPC (Fig. S5 and Table 4). Therefore, the AtLYSOPL2 catalytic triad mutant proteins (S147A, D268A, and H298A) were used to measure the thermodynamic parameters for lysoPC binding. The weak interactions between the AtLYSOPL2 catalytic triad mutant proteins (S147A, D268A, and H298A) and lysoPC were reflected in an exothermic heat burst with K_D values of 101.72, 99.67, and 137.37 μM, respectively (Table 4). Unlike the AtACBP2–AtLYSOPL2 interaction, the thermodynamic forces from the AtLYSOPL2 catalytic triad mutant protein–lysoPC interactions were driven by a change in both enthalpy (ΔH) and entropy ($-T\Delta S$) (Fig. 6*B*), indicating that hydrogen bonding and hydrophobic forces contribute to the interaction of AtLYSOPL2 with lysoPC.

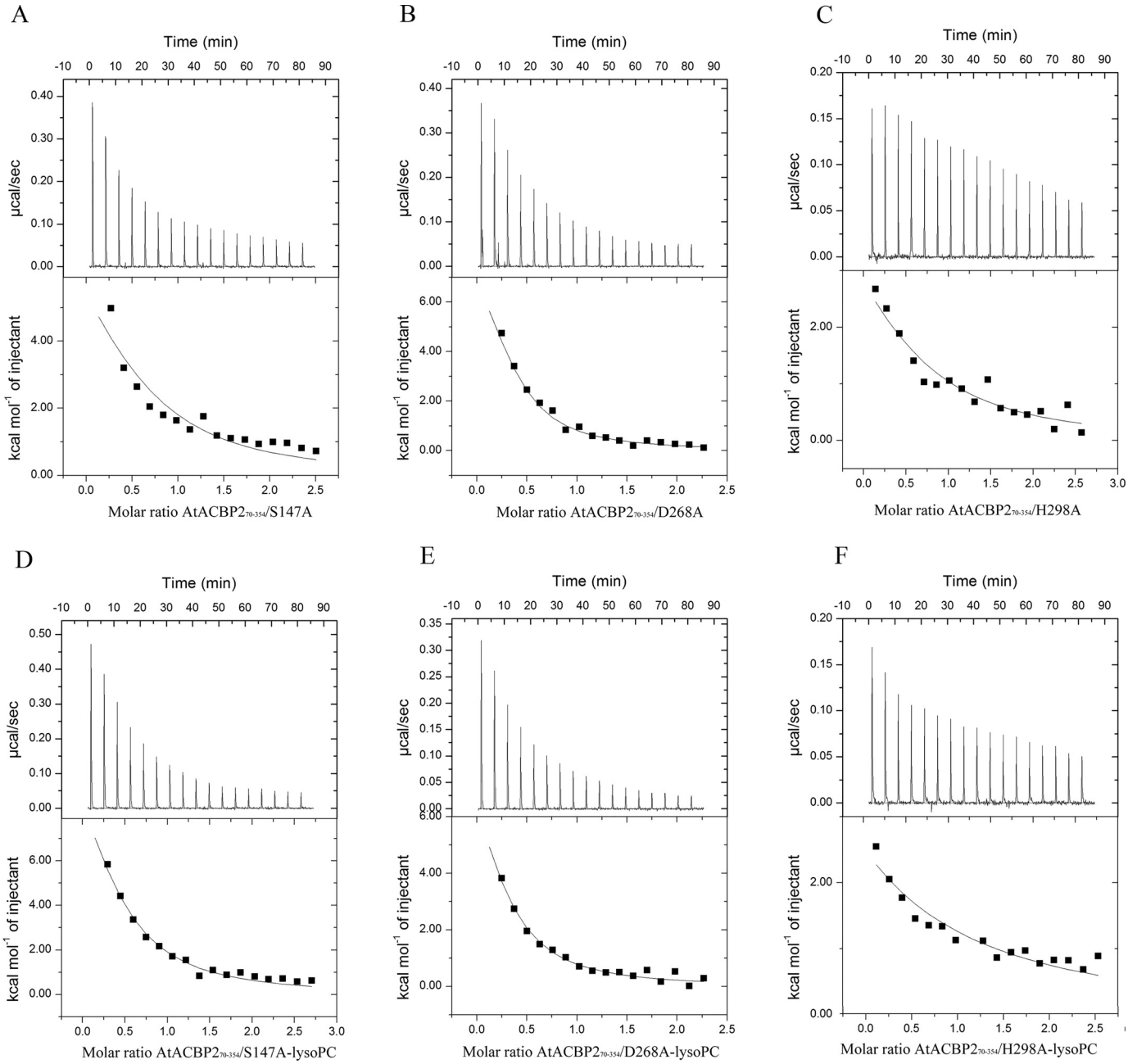

Figure 5. ITC analysis of interactions between AtACBP2$_{70-354}$ and AtLYSOPL2 mutant proteins in the absence or presence of lysoPC. *A–C*, AtACBP2$_{70-354}$ interactions with AtLYSOPL2 mutants S147A (*A*), D268A (*B*), and H298A (*C*) in the absence of lysoPC. Interactions were measured by titrating 20–30 μM AtLYSOPL2 (S147A, D268A, and H298A) in the chamber with 300–400 μM AtACBP2$_{70-354}$ in the syringe. *D–F*, AtACBP2$_{70-354}$ interactions with AtLYSOPL2 mutants S147A (*D*), D268A (*E*), H298A (*F*) in the presence of lysoPC. Interactions were measured by titrating 30 μM AtLYSOPL2 (S147A, D268A, and H298A)–lysoPC complex (molar ratio 1:1) in the chamber with 400–500 μM AtACBP2$_{70-354}$ in the syringe. *Top panel*, raw heating power over time; *bottom panel*, fit of the integrated energy values normalized for the injected protein. The values originate from Table 2.

Discussion

Studies on lysophospholipases in bacteria, yeasts, and mammals suggest that these enzymes play a major role in LPL degradation (37, 38). In contrast, very few reports are available on plant lysophospholipases. Structural alignments on lysophospholipases indicate that they share a very conserved hydrolase tertiary structure, arising from convergent evolution, and hydrolase action is conserved among various species. AtLYSOPL2 belongs to the serine hydrolase superfamily (19), and several crystal structures of its homologues, including *Serratia marcescens* lipase lipA, *Ophiostoma piceae* sterol esterase, and human MGL, have been reported (21, 39, 40). As homology models are useful in examining ligand binding in many proteins, this strategy was used in the structural prediction of AtLYSOPL2 (Fig. 3).

Although the lysoPC-hydrolyzing activity (Fig. 4) of AtLYSOPL2 (19) has been confirmed by an independent group (41), this protein has also been identified as a caffeoyl shikimate esterase (22), suggesting that AT1G52760 is a multifunctional enzyme. In fact, the Ser–Asp–His catalytic triad, which is critical for the lysophospholipase (19, 20) and esterase activities

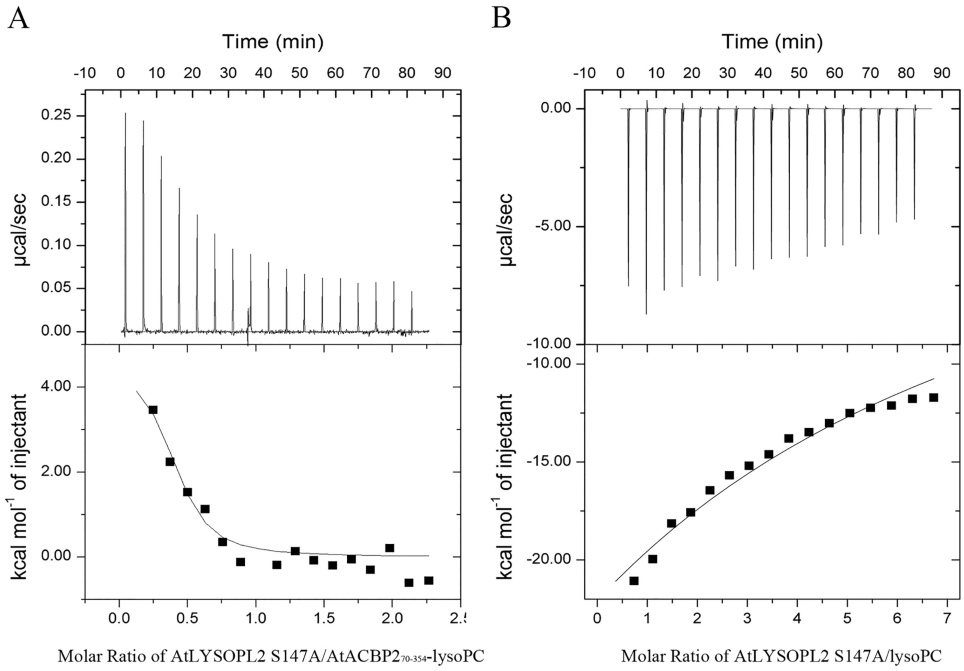

Figure 6. ITC analysis of AtLYSOPL2 catalytic triad mutant S147A interactions with the AtACBP2$_{70-354}$–lysoPC complex and lysoPC. *A,* binding of AtLYSOPL2 S147A and AtACBP2$_{70-354}$–lysoPC complex was measured by titrating 20–30 μM AtLYSOPL2 S147A in the chamber with 400–500 μM of the AtACBP2$_{70-354}$–lysoPC (molar ratio 1:1) complex in the syringe. *B,* AtLYSOPL2 S147A and lysoPC interaction was measured by titrating 20–30 μM AtLYSOPL2 S147A in the chamber with 600–800 μM lysoPC in the syringe. *Top panel*, raw heating power over time; *bottom panel*, fit of the integrated energy values normalized for the injected protein. The values originate from Tables 3 and 4.

Table 3

ITC binding constants and thermodynamic parameters for interactions of AtLYSOPL2 wildtype, or mutant proteins with truncated AtACBP2 proteins with/without lysoPC

The values are plotted in Fig. 6 and Fig. S4. AtACBP2$_{70-214}$ and AtACBP2$_{215-354}$ represent AtACBP2 lacking ankyrin repeats and AtACBP2 lacking the acyl-CoA–binding domain, respectively. Experiments were carried out at 25 °C, and each value is the mean of at least three independent titrations. *n* is number of binding sites (*n* = ligand/receptor); K_D is dissociation constant; ΔH is enthalpy change; ΔS is entropy change; ΔG is Gibbs free energy. The binding entropy and enthalpy determine ligand binding. Positive is unfavorable, and negative is favorable (61, 62). ND indicates not determinable values due to lack of binding.

Combinations	*n*	K_D	ΔH	$-T\Delta S$	ΔG
		μM	kcal mol^{-1}	kcal mol^{-1}	kcal mol^{-1}
Wildtype AtLYSOPL2					
with AtACBP2$_{70-354}$-lysoPC	0.89 ± 0.27	33.48 ± 0.08	9.38 ± 0.20	−15.14 ± 0.65	−5.76 ± 0.68
with AtACBP2$_{70-354}$	1.05 ± 0.01	28.98 ± 3.36	9.55 ± 0.26	−15.38 ± 0.13	−5.93 ± 0.12
with AtACBP2$_{70-214}$-lysoPC	ND	ND	ND	ND	ND
with AtACBP2$_{70-214}$	ND	ND	ND	ND	ND
with AtACBP2$_{215-354}$-lysoPC	ND	ND	ND	ND	ND
with AtACBP2$_{215-354}$	ND	ND	ND	ND	ND
AtLYSOPL2 S147A					
with AtACBP2$_{70-354}$-lysoPC	0.38 ± 0.08	1.69 ± 0.11	4.85 ± 1.5	−12.46 ± 0.12	−7.88 ± 1.5
with AtACBP2$_{70-354}$	0.56 ± 0.17	20.7 ± 1.03	10.71 ± 3.19	−15.7 ± 3.21	−4.99 ± 2.2
with AtACBP2$_{70-214}$-lysoPC	ND	ND	ND	ND	ND
with AtACBP2$_{70-214}$	ND	ND	ND	ND	ND
with AtACBP2$_{215-354}$-lysoPC	ND	ND	ND	ND	ND
with AtACBP2$_{215-354}$	ND	ND	ND	ND	ND
AtLYSOPL2 D268A					
with AtACBP2$_{70-354}$-lysoPC	0.53 ± 0.02	1.38 ± 0.42	5.10 ± 0.16	−13.68 ± 0.20	−8.58 ± 0.26
with AtACBP2$_{70-354}$	0.37 ± 0.08	12.39 ± 0.24	9.27 ± 1.16	−15.94 ± 1.18	−6.67 ± 1.4
with AtACBP2$_{70-214}$-lysoPC	ND	ND	ND	ND	ND
with AtACBP2$_{70-214}$	ND	ND	ND	ND	ND
with AtACBP2$_{215-354}$-lysoPC	ND	ND	ND	ND	ND
with AtACBP2$_{215-354}$	ND	ND	ND	ND	ND
AtLYSOPL2 H298A					
with AtACBP2$_{70-354}$-lysoPC	0.61 ± 0.06	0.89 ± 0.05	4.98 ± 0.06	−13.69 ± 1.35	−8.71 ± 1.35
with AtACBP2$_{70-354}$	0.84 ± 0.03	25.64 ± 0.17	6.42 ± 1.2	−12.67 ± 1.45	−5.27 ± 1.84
with AtACBP2$_{70-214}$-lysoPC	ND	ND	ND	ND	ND
with AtACBP2$_{70-214}$	ND	ND	ND	ND	ND
with AtACBP2$_{215-354}$-lysoPC	ND	ND	ND	ND	ND
with AtACBP2$_{215-354}$	ND	ND	ND	ND	ND

(22) of AT1G52760, is conserved to catalyze lysophospholipase and esterase activities of other multifunctional enzymes, such as the *Escherichia coli* thioesterase I, also known as protease I and phospholipase L1 (EC 3.1.2.2) (42). Vijayaraj *et al.* (41) confirmed that AT1G52760 is a bifunctional enzyme with broad substrate specificities. Moreover, the hydrolase activity

Table 4

ITC binding constants and thermodynamic parameters for interactions of AtLYSOPL2 wildtype or mutant proteins with lysoPC

The values are plotted in Fig. 6 and Fig. S5. Experiments were carried out at 25 °C, and each value is the mean of at least three independent titrations. *n* is number of binding sites (*n* = ligand/receptor); K_D is dissociation constant; ΔH is enthalpy change; ΔS is entropy change; ΔG is Gibbs free energy. The binding entropy and enthalpy determine ligand binding. Positive is unfavorable ,and negative is favorable (61, 62). ND indicates not determinable values due to lack of binding.

Combinations	*n*	K_D	ΔH	$-T\Delta S$	ΔG
		μM	*kcal mol*$^{-1}$	*kcal mol*$^{-1}$	*kcal mol*$^{-1}$
Wildtype AtLYSOPL2/lysoPC	ND	ND	ND	ND	ND
AtLYSOPL2 S147A/lysoPC	1.08 ± 0.03	101.72 ± 0.19	−1.67 ± 0.05	−13.44 ± 0.40	−15.11 ± 0.41
AtLYSOPL2 D268A/lysoPC	0.92 ± 0.03	99.67 ± 0.05	−1.66 ± 0.01	−9.56 ± 0.20	−11.21 ± 0.20
AtLYSOPL2 H298A/lysoPC	1.02 ± 0.01	137.37 ± 0.11	−1.68 ± 0.01	−10.85 ± 0.38	−12.52 ± 0.38

of AT1G52760 is supported by the occurrence of the Gly–Xaa–Ser–Xaa–Gly lipase motif conserved among the 16 AtMAGL members and the His–Xaa_4–Asp acyltransferase motif conserved in some other AtMAGLs (20, 41). Besides the *in vitro* enzyme assays, we have previously demonstrated the physiological role for AtLYSOPL2 in phospholipid repair following lipid peroxidation under metal-induced stress *in planta* using *Arabidopsis* mutants and overexpressors (19), in agreement with the observation that AT1G52760 is a membrane-associated protein by confocal laser-scanning microscopy (19, 20).

In site-directed mutagenesis experiments on *Rattus norvegicus* MGL and *Mus musculus* lysophospholipase (lysoPLA I), the catalytic triad (Ser–His–Asp) was shown to be essential for lipase activities (37, 38, 43). Like the mRNA encoding MGL that is ubiquitously expressed in all tissues (43), *AtLYSOPL2* mRNA was detected in roots, stems, and flowers (19), particularly higher in roots and stems than other organs (20). Its protein was observed to accumulate in *Arabidopsis* roots (Fig. S6). Similar to murine lysoPLA I, which has been proposed to function in the removal of LPLs produced by murine phospholipase A_1 and A_2 (37), AtLYSOPL2 contains an α/β hydrolase fold and may share similar roles in lysoPC removal by phospholipase hydrolysis.

Besides Ser-147, which is located in the conserved G*X*S*X*G motif, the other two conserved catalytic residues (Asp-268 and His-298) of AtLYSOPL2 were also proven essential for lysophospholipase activity (Fig. 4). LysoPC was not efficiently cleaved by the AtLYSOPL2 mutant proteins S147A, D268A, and H298A in GC-MS assays (Fig. 4). In this respect, AtLYSOPL2 resembles *R. norvegicus* MGL of which substitutions in the corresponding residues rendered it ineffective (21, 38, 43).

Thermodynamic analysis by ITC was carried out to study the relationship between lysoPC and its target protein complex ($AtACBP2_{70-354}$–AtLYSOPL2) and demonstrated that $AtACBP2_{70-354}$ binds to AtLYSOPL2 and lysoPC with similar K_D values, both in the micromolar concentration range (Fig. S7). Although the crystal structures of the lysoPC-bound states have not been solved with either AtACBP2 or AtLYSOPL2, a common feature was observed based on thermodynamic analysis on $AtACBP2_{70-354}$ binding to AtLYSOPL2 and lysoPC. Their interactions were endothermic and were driven solely by a large change in entropy ($-T\Delta S$), which usually suggests that conformational change and hydrophobicity are the main driving forces in such interactions. A large amount of ordered water molecules localized on the hydrophobic interfaces of the binding molecules that are disseminated into the bulk solvent drive the hydrophobic interactions, and conformational changes of binding molecules occur accompanied by release of water molecules (44). Our results suggest that the interactions of $AtACBP2_{70-354}$ to lysoPC and $AtACBP2_{70-354}$ to AtLYSOPL2 led to conformational changes to form hydrophobic binding surfaces, which associate with the dissipation of water molecules. Interestingly, the binding affinity of $AtACBP2_{70-354}$ premixed with lysoPC to AtLYSOPL2 mutants S147A, D268A, or H298A (K_D = 1.69, 1.38, and 0.89 μM, respectively) were 12-, 21-, and 25-fold higher than the binding affinity of unliganded $AtACBP2_{70-354}$ to AtLYSOPL2 mutants S147A, D268A, or H298A (K_D = 20.7, 12.39, and 25.64 μM, respectively) (Table 3). These results argue that the conformational change caused by $AtACBP2_{70-354}$ binding to lysoPC enhanced the hydrophobic interaction of $AtACBP2_{70-354}$ with AtLYSOPL2 mutants (S147A, D268A, or H298A) (Fig. 6*A* and Table 3). Hence, it appears that the $AtACBP2_{70-354}$–lysoPC interaction could strengthen the hydrophobic interaction between $AtACBP2_{70-354}$ and AtLYSOPL2. Similarly, the type 2C protein phosphatases (PP2Cs) are considered to be co-receptors in the abscisic acid (ABA)-signaling transduction pathway because their presence improved ABA perception by the ABA receptor protein family, PYRABACTIN RESISTANCE1(PYR1)/PYR1-like(PYL)/regulatory components of ABA receptor (RCAR) (PYR/PYL/RCAR) (45, 46). The availability of protein surfaces arising from conformational changes upon the interaction of PYR/PYL/RCAR to ABA promoted the binding of ABA to PP2Cs (45, 46).

In contrast, the binding of AtLYSOPL2 mutants S147A, D268A, or H298A to lysoPC was exothermic with weak binding affinities of K_D values of 101.72, 99.67, and 137.37 μM, respectively (Fig. 6*B* and Table 4). The lower binding affinity of lysoPC to AtLYSOPL2 mutants (S147A, D268A, or H298A), which compared with the $AtACBP2_{70-354}$–lysoPC complex to S147A, D268A, or H298A, suggests that AtLYSOPL2 interaction with $AtACBP2_{70-354}$ benefits from the pre-binding of $AtACBP2_{70-354}$ to lysoPC. In other words, $AtACBP2_{70-354}$ likely plays a role in facilitating AtLYSOPL2 and lysoPC interactions (Fig. S7). Consistently, it has been recently demonstrated that site-directed mutagenesis of AtACBP1 (Y171A), a homologue of AtACBP2, weakened its interaction with STEROL C4-METHYL OXIDASE1 *in vivo* (47, 48). Thus, it appears to be a general observation that the liganded state of AtACBP1 (47, 48) and AtACBP2 (this study) promotes their association with protein partners, accounting for the essence of both the ankyrin repeats and the acyl-CoA–binding domain for protein–protein interactions (Fig. S4 and Table 3).

Binding of acyl-CoA thioesters to AtACBP2$_{70-354}$ was favored by both entropy and enthalpy, indicating that hydrogen bonding and hydrophobic forces supported the interaction. The thermodynamic analysis obtained here is consistent with data from analyses on the co-crystal structure of human cytosolic liver ACBP with myristoyl-CoA (49). Conserved positively-charged residues (Tyr-29, Lys-33, and Lys-55) in hL-ACBP form hydrogen bonds with the 3′-phosphate moiety in myristoyl-CoA, whereas a hydrophobic groove in hL-ACBP interacts with the hydrophobic acyl moiety (49). Meanwhile, lysoPC is composed of a hydrophilic head (glycerol 3-phosphocholine) and a hydrophobic fatty acid tail that should be crucial in binding AtACBP2, as the hydrophobic force mainly contributes to interaction of AtACBP2 with lysoPC from ITC analysis. However, the interaction of AtLYSOPL2 and lysoPC was favored by both entropy ($-T\Delta S$) and enthalpy (ΔH). Thus, both the hydrophilic head and hydrophobic fatty acid tail of lysoPC are important for the weak interaction of lysoPC with AtLYSOPL2.

AtACBP2 contains a transmembrane domain, whereas AtLYSOPL2 possesses a lysoPC interactive hydrophobic region that is potentially involved in membrane binding, suggesting that AtACBP2 and AtLYSOPL2 perform their biological functions at cellular membranes (19). An *Arabidopsis* patatin-related phospholipase, pPLAIIIβ, was reported to be associated with the plasma membrane (50), resembling the co-localization of AtACBP2 and AtLYSOPL2 at the plasma membrane (19). pPLAIIIβ also accumulated in *Arabidopsis* roots resembling AtLYSOPL2 and is thus considered to act upstream of AtLYSOPL2 and AtACBP2 (50). LysoPC is a major signaling molecule in cellular membranes produced by phospholipases (3), in response to environmental stresses (6, 7). Taken together, the *in vitro* thermodynamic data suggest that AtACBP2 binds lysoPC to facilitate AtLYSOPL2 action following environmental stimuli (Fig. 7).

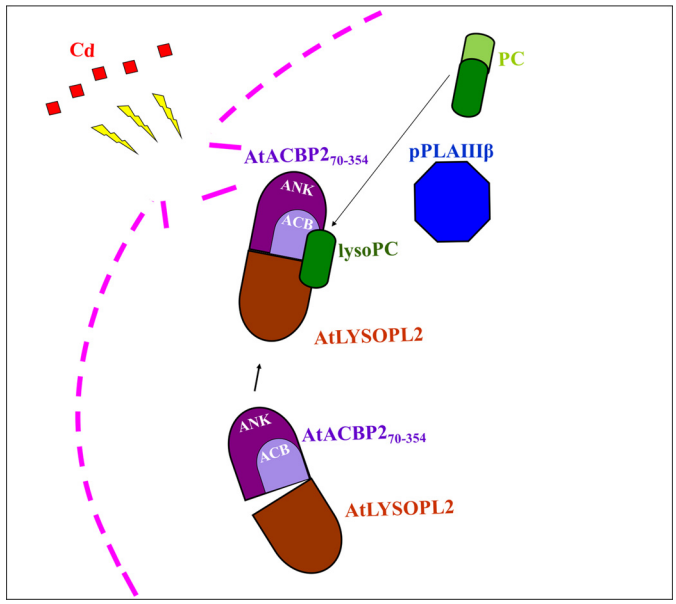

Figure 7. Proposed working model for AtLYSOPL2, AtACBP2, and lysoPC interaction. LysoPC, generated by pPLAIIIβ action on phosphatidylcholine (PC), binds to AtACBP2 and promotes the formation of an AtLYSOPL2–AtACBP2 complex. This complex could improve efficiency in membrane repair following Cd-induced stress. Cd, *red*; plasma membrane, *pink*; lysoPC, *dark green*; PC, *light green*; ankyrin-repeat (ANK) domain, *purple*; acyl-CoA-binding (ACB) domain, *light purple*; PLAIII β, *blue*; AtLYSOPL2, *brown*.

Experimental procedures

Generation of protein expression constructs

All primers are listed in Table S1. The *AtLYSOPL2* and *AtACBP2* cDNA fragments were amplified from plasmids pAT426 (19) and pAT377 (19), respectively, by PCR using Q5® high-fidelity polymerase (New England Biolabs) with denaturation at 95 °C for 5 min, followed by 31 cycles of 94 °C for 30 s, 55 °C for 30 s, and 72 °C for 1 min 30 s, and an extension at 72 °C for 10 min. Site-directed mutagenesis of *AtLYSOPL2* cDNA was performed according to Ho *et al.* (51). Overlapping forward and reverse oligonucleotide primers were designed at the target point mutation sites (Table S1). The PstI/NcoI-digested fragments encoding WT, D268A, H298A, and S147A AtLYSOPL2 (corresponding to aa 1–332) were inserted into the pRSETAHisSUMO expression vector (52) to generate plasmids pAT670, pAT780, pAT781, and pAT798, respectively. The AgeI/HindIII fragment encoding AtACBP2$_{70-354}$ (corresponding to aa 70–354, inclusive of the acyl-CoA–binding domain and the ankyrin repeats) was inserted into the pRSETAHisSUMO vector (52) to generate plasmid pAT672. The 435-bp cDNA fragment encoding AtACBP2$_{70-214}$ (corresponding to aa 70–214, inclusive of the acyl-CoA–binding domain) and the 421-bp fragment encoding AtACBP2$_{215-354}$ (corresponding to aa 215–354 inclusive of the ankyrin repeats) were amplified from plasmid pAT672 and cloned into the pGEM®-T Easy vector (Promega) to generate plasmids pAT939 and pAT940, respectively. The BamHI/HindIII fragment and EcoRI/HindIII fragment were excised from pAT939 and pAT940 and inserted into the pRSETAHisSUMO vector (52) to generate plasmids pAT941 and pAT942, respectively. All plasmids were used for *E. coli* DH5α transformation. The transformants harboring the *AtLYSOPL2* and *AtACBP2* constructs were screened by colony-PCR using the T7/ML2041 and T7/ML2039 primer pairs, respectively. All constructs were verified by DNA sequencing across the cloning sites to ensure in-frame protein expression with the polyhistidine tag.

Protein expression

E. coli BL21 (DE3) pLysS was transformed with plasmids pAT670, pAT672, pAT780, pAT781, pAT798, pAT941, and pAT942. Transformants were selected on LB agar plates supplemented with 100 μg/ml ampicillin and 34 μg/ml chloramphenicol. Ten single colonies per transformation were screened for the highest protein expression. A single colony of the high-expression clone was used to inoculate 50 ml of LB medium containing 100 μg/ml ampicillin and 34 μg/ml chloramphenicol and incubated with shaking overnight at 220 rpm at 37 °C. The pre-culture was used to inoculate 4 liters of LB medium supplemented with 100 μg/ml ampicillin and 34 μg/ml chloramphenicol at 1:100 dilution. When the culture reached an OD$_{600}$ value of 0.6, isopropyl β-D-thiogalactopyranoside was added to a final concentration of

0.8 mM. The culture was grown for 16 h at 220 rpm at 16 °C for recombinant AtLYSOPL2 and 24 °C for recombinant AtACBP2. Cells were harvested by centrifugation at 9,000 rpm at 4 °C for 5 min. The cell pellet was used immediately or stored in −80 °C.

Protein purification

The cell pellet was resuspended in buffer A (20 mM Tris-HCl, pH 7.5, 500 mM NaCl, 50 mM imidazole). After sonication, the cell lysate was centrifuged at 18,000 × *g* at 4 °C for 50 min to spin down the cell debris. The cell-free extract was applied onto a buffer A-equilibrated nickel (Ni)-charged resin column. After washing with 10 column volumes of buffer A, buffer B (20 mM Tris-HCl, pH 7.5, 500 mM NaCl, 300 mM imidazole) was used to elute recombinant AtLYSOPL2 WT protein, AtLYSOPL2 mutant proteins (S147A, D268A, and H298A), and AtACBP2$_{70-354}$ protein. Buffer B eluate was collected. Dialysis was conducted using dialysis buffer (20 mM Tris-HCl, pH 7.5, 100 mM NaCl) to remove imidazole. SUMO protease was applied at the same time to cleave the HisSUMO tag from the target protein. The dialyzed solution was applied onto a Ni-charged resin column again to remove the cleaved HisSUMO tag and SUMO protease. AtLYSOPL2 WT protein, AtLYSOPL2 mutant proteins (S147A, D268A, and H298A), and AtACBP2$_{70-354}$ protein were collected from the flow-through fraction.

Western blot analysis

The protein assay kit from Bio-Rad was used to estimate total protein separated on an SDS-polyacrylamide gel before electrophoretic transfer to the Hybond-C membrane (Amersham Biosciences) by the Trans-Blot Turbo Transfer System (Bio-Rad). Twenty μg of total protein was loaded per well in an SDS-polyacrylamide gel. AtLYSOPL2-specific antibodies generated previously in rabbits using a synthetic peptide (REWIDEKVKKYGSKT) corresponding to aa 317–331 of AtLYSOPL2 (19) were used to identify the AtLYSOPL2 cross-reacting bands in Western blot analysis. The ECL Western blotting detection kit (Amersham Biosciences) was used for detection of cross-reacting bands in Western blot analysis.

Lysophospholipase activity assays

LysoPC (C16:0) from soybean (Avanti Polar Lipids Inc.) was used as a substrate for measuring lysophospholipase activities by GC-MS following previous methods with modification (53, 54). Purified AtLYSOPL2 (50 μg) was assayed in 1 ml of reaction mixture containing 50 mM potassium-phosphate buffer, pH 8.0, 100 μM substrate, and 0.2% (v/v) Triton X-100. Gum arabic (5% w/v) was used to emulsify the substrate by sonication for 30 s before addition of AtLYSOPL2. The reaction was performed at 33 °C for 1 h with 100-μl aliquots withdrawn at 10-min intervals. Free fatty acids were purified from the reaction mixtures by TLC, and fatty acid methyl esters were prepared by methanolysis at 80 °C for 3 h in 5% (v/v) HCl/methanol, extracted with hexane, and then quantified by a trace GC-polaris Q mass spectrometer (Finnigan-Spectronex, ThermoFisher Scientific), equipped with a DB-5 column (30 m × 0.25 film thickness; J&W Scientific, Folsom, CA), following a temperature program described previously (55).

ITC measurements

The experiments were conducted using a MicroCal ITC200 system (GE Healthcare). Purified recombinant proteins were dialyzed against a buffer containing 20 mM Tris (pH 7.5) and 20 mM NaCl before ITC. AtACBP2$_{70-354}$ (0.4–0.5 mM), AtACBP2$_{70-214}$ lacking ankyrin repeats (0.4–0.5 mM), AtACBP2$_{215-354}$ lacking the acyl-CoA–binding domain (0.4 mM), a mixture of AtACBP2$_{70-354}$ with lysoPC (C16:0) (molar ratio 1:1), AtACBP2$_{70-214}$–lysoPC complex (molar ratio 1:1), or AtACBP2$_{215-35-}$lysoPC complex (molar ratio 1:1) was titrated automatically into a solution of AtLYSOPL2 WT protein, AtLYSOPL2 mutant proteins (S147A, D268A, and H298A) (30–40 μM), a mixture of AtLYSOPL2 with lysoPC (C16:0) (molar ratio 1:1), or a mixture of each AtLYSOPL2 mutant protein with lysoPC (C16:0), respectively. The interactions of AtACBP2$_{70-354}$ with lysoPC (C16:0) and C16:0–CoA (Avanti Polar Lipids Inc.) were also performed by ITC. AtACBP2$_{70-354}$ and C16:0–CoA interaction was measured by titrating 30–40 μM AtACBP2$_{70-354}$ in the chamber with 0.6–0.8 mM C16:0–CoA in the syringe. For AtACBP2$_{70-354}$ and lysoPC interaction, 30–40 μM AtACBP2$_{70-354}$ in the chamber was titrated with 0.6–0.8 mM lysoPC in the syringe, and the dialysis buffer was supplemented with 5% (v/v) acetonitrile (56). The interactions of AtLYSOPL2 WT protein or AtLYSOPL2 mutant proteins (S147A, D268A, and H298A) and lysoPC (C16:0) were each measured by titrating 30–40 mM AtLYSOPL2 WT protein or AtLYSOPL2 mutant proteins (S147A, D268A, and H298A) in the chamber with 0.6–0.8 mM lysoPC in the syringe, and the dialysis buffer was also mixed with 5% (v/v) acetonitrile. Typically, each injection was performed at 25 °C with 17 injections of 2-μl aliquots of the ligand into the protein solution (250 μl in the cell) at 300-s intervals. The association constant (K_A), binding stoichiometry (n), and enthalpy changes (ΔH) upon binding were derived directly, and the Gibbs energy (ΔG) and entropy ($-T\Delta S$) changes were calculated from the equation, $\Delta G^0 = \Delta H^0 - T\Delta S^0 = -RT\ln K_A$. Data were collected and analyzed using the ORIGIN software version 7.0 (MicroCal).

Homology modeling and dock simulation

The tertiary structural model of AtLYSOPL2 was created using the software MODELLER version 9.14. The X-ray crystal structure of human MGL (Protein Data Bank code 3JW8) served as a template for homology modeling (57–59). The lysoPC-binding pocket was identified using automated ligand docking by the software AutoDock version 4.0 (http://autodock.scripps.edu/)[3] (60). The ligand of lysoPC (C16:0) was generated by the software ChemDraw version 8.0. The program allowed the ligand to be flexible, whereas the side chains in the protein were fixed. The grid box covered the entire protein of AtLYSOPL2. The ligand lysoPC (C16:0) was then docked using genetic algorithm/local search hybrid simulation. The lowest energy configuration was assumed to be the best docking pose for AtLYSOPL2.

Author contributions—R. M., X. D. L., and M.-L. C. conceptualization; X. D. L. and M.-L. C. resources; R. M., S.-C. L., X. L., X. D. L., and M.-L. C. data curation; R. M. and M.-L. C. software; R. M., S.-C. L., X. L., X. D. L., and M.-L. C. formal analysis; R. M., S.-C. L., X. D. L., and M.-L. C. validation; R. M., S.-C. L., X. L., X. D. L., and M.-L. C. investigation; R. M., S.-C. L., X. D. L., and M.-L. C. visualization; R. M., S.-C. L., X. L., X. D. L., and M.-L. C. methodology; R. M., X. D. L., and M.-L. C. writing-original draft; R. M. and M.-L. C. project administration; R. M., S.-C. L., X. D. L., and M.-L. C. writing-review and editing; X. D. L. and M.-L. C. supervision; M.-L. C. funding acquisition.

Acknowledgments—We are grateful to Wing-Ki Chan for technical support and Prof. Kam-Bo Wong for gift of the pRSETAHisSUMO vector.

References

1. de Kroon, A. I., Rijken, P. J., and De Smet, C. H. (2013) Checks and balances in membrane phospholipid class and acyl chain homeostasis, the yeast perspective. *Prog. Lipid Res.* **52,** 374–394 CrossRef Medline
2. Grechkin, A. (1998) Recent developments in biochemistry of the plant lipoxygenase pathway. *Prog. Lipid Res.* **37,** 317–352 CrossRef Medline
3. Wang, X. (2004) Lipid signaling. *Curr. Opin. Plant Biol.* **7,** 329–336 CrossRef Medline
4. Ryu, S. B. (2004) Phospholipid-derived signaling mediated by phospholipase A in plants. *Trends Plant Sci.* **9,** 229–235 CrossRef Medline
5. Welti, R., Li, W., Li, M., Sang, Y., Biesiada, H., Zhou, H. E., Rajashekar, C. B., Williams, T. D., and Wang, X. (2002) Profiling membrane lipids in plant stress responses: role of phospholipase Dα in freezing-induced lipid changes in *Arabidopsis*. *J. Biol. Chem.* **277,** 31994–32002 CrossRef Medline
6. D'Arrigo, P., and Servi, S. (2010) Synthesis of lysophospholipids. *Molecules* **15,** 1354–1377 CrossRef Medline
7. Torkhovskaya, T. I., Ipatova, O. M., Zakharova, T. S., Kochetova, M. M., and Khalilov, E. M. (2007) Lysophospholipids receptors in cell signaling. *Biochemistry* **72,** 125–131 Medline
8. Wi, S. J., Seo, Sy., Cho, K., Nam, M. H., and Park, K. Y. (2014) Lysophosphatidylcholine enhances susceptibility in signaling pathway against pathogen infection through biphasic production of reactive oxygen species and ethylene in tobacco plants. *Phytochemistry* **104,** 48–59 CrossRef Medline
9. Moolenaar, W. H. (2000) Development of our current understanding of bioactive lysophospholipids. *Ann. N.Y. Acad. Sci.* **905,** 1–10 Medline
10. Asaoka, Y., Oka, M., Yoshida, K., Sasaki, Y., and Nishizuka, Y. (1992) Role of lysophosphatidylcholine in T-lymphocyte activation: involvement of phospholipase A2 in signal transduction through protein kinase C. *Proc. Natl. Acad. Sci. U.S.A.* **89,** 6447–6451 CrossRef Medline
11. Murohara, T., Scalia, R., and Lefer, A. M. (1996) Lysophosphatidylcholine promotes P-selectin expression in platelets and endothelial cells: possible involvement of protein kinase C activation and its inhibition by nitric oxide donors. *Circ. Res.* **78,** 780–789 CrossRef Medline
12. Wuhanqimuge, Itakura, A., Matsuki, Y., Tanaka, M., and Arioka, M. (2013) Lysophosphatidylcholine enhances NGF-induced MAPK and Akt signals through the extracellular domain of TrkA in PC12 cells. *FEBS Open Bio.* **3,** 243–251 CrossRef Medline
13. Makide, K., Uwamizu, A., Shinjo, Y., Ishiguro, J., Okutani, M., Inoue, A., and Aoki, J. (2014) Novel lysophospholipid receptors: their structure and function. *J. Lipid Res.* **55,** 1986–1995 CrossRef Medline
14. McIntyre, T. M., Pontsler, A. V., Silva, A. R., St Hilaire, A., Xu, Y., Hinshaw, J. C., Zimmerman, G. A., Hama, K., Aoki, J., Arai, H., and Prestwich, G. D. (2003) Identification of an intracellular receptor for lysophosphatidic acid (LPA): LPA is a transcellular PPARγ agonist. *Proc. Natl. Acad. Sci. U.S.A.* **100,** 131–136 CrossRef Medline
15. Pasternack, S. M., von Kügelgen, I., Al Aboud, K., Lee, Y. A., Rüschendorf, F., Voss, K., Hillmer, A. M., Molderings, G. J., Franz, T., Ramirez, A., Nürnberg, P., Nothen, M. M., and Betz, R. C. (2008) G protein-coupled receptor P2Y5 and its ligand LPA are involved in maintenance of human hair growth. *Nat. Genet.* **40,** 329–334 CrossRef Medline
16. Kawaguchi, M., Okabe, T., Okudaira, S., Hanaoka, K., Fujikawa, Y., Terai, T., Komatsu, T., Kojima, H., Aoki, J., and Nagano, T. (2011) Fluorescence probe for lysophospholipase C/NPP6 activity and a potent NPP6 inhibitor. *J. Am. Chem. Soc.* **133,** 12021–12030 CrossRef Medline
17. Wang, A., and Dennis, E. A. (1999) Mammalian lysophospholipases. *Biochim. Biophys. Acta* **1439,** 1–16 CrossRef Medline
18. de Torres Zabela, M., Fernandez-Delmond, I., Niittyla, T., Sanchez, P., and Grant, M. (2002) Differential expression of genes encoding *Arabidopsis* phospholipases after challenge with virulent or avirulent *Pseudomonas* isolates. *Mol. Plant Microbe Interact.* **15,** 808–816 CrossRef Medline
19. Gao, W., Li, H. Y., Xiao, S., and Chye, M. L. (2010) Acyl-CoA-binding protein 2 binds lysophospholipase 2 and lysoPC to promote tolerance to cadmium-induced oxidative stress in transgenic *Arabidopsis*. *Plant J.* **62,** 989–1003 Medline
20. Kim, R. J., Kim, H. J., Shim, D., and Suh, M. C. (2016) Molecular and biochemical characterizations of the monoacylglycerol lipase gene family of *Arabidopsis thaliana*. *Plant J.* **85,** 758–771 CrossRef Medline
21. Bertrand, T., Augé, F., Houtmann, J., Rak, A., Vallée, F., Mikol, V., Berne, P. F., Michot, N., Cheuret, D., Hoornaert, C., and Mathieu, M. (2010) Structural basis for human monoglyceride lipase inhibition. *J. Mol. Biol.* **396,** 663–673 CrossRef Medline
22. Vanholme, R., Cesarino, I., Rataj, K., Xiao, Y., Sundin, L., Goeminne, G., Kim, H., Cross, J., Morreel, K., Araujo, P., Welsh, L., Haustraete, J., McClellan, C., Vanholme, B., Ralph, J., *et al.* (2013) Caffeoyl shikimate esterase (CSE) is an enzyme in the lignin biosynthetic pathway in *Arabidopsis*. *Science* **341,** 1103–1106 CrossRef Medline
23. Gao, W., Xiao, S., Li, H. Y., Tsao, S. W., and Chye, M. L. (2009) *Arabidopsis thaliana* acyl-CoA–binding protein ACBP2 interacts with heavy-metal–binding farnesylated protein AtFP6. *New Phytol.* **181,** 89–102 CrossRef Medline
24. Clemens, S. (2006) Toxic metal accumulation, responses to exposure and mechanisms of tolerance in plants. *Biochimie* **88,** 1707–1719 CrossRef Medline
25. Wong, C. K. E., and Cobbett, C. S. (2009) HMA P-type ATPases are the major mechanism for root-to-shoot Cd translocation in *Arabidopsis thaliana*. *New Phytol.* **181,** 71–78 CrossRef
26. Clemens, S., and Ma, J. F. (2016) Toxic heavy metal and metalloid accumulation in crop plants and foods. *Annu. Rev. Plant Biol.* **67,** 489–512 CrossRef Medline
27. Park, J., Song, W. Y., Ko, D., Eom, Y., Hansen, T. H., Schiller, M., Lee, T. G., Martinoia, E., and Lee, Y. (2012) The phytochelatin transporters AtABCC1 and AtABCC2 mediate tolerance to cadmium and mercury. *Plant J.* **69,** 278–288 CrossRef Medline
28. Khairnar, N. P., Joe, M. H., Misra, H. S., Lim, S. Y., and Kim, D. H. (2013) FrnE, a cadmium-inducible protein in *Deinococcus radiodurans*, is characterized as a disulfide isomerase chaperone *in vitro* and for its role in oxidative stress tolerance *in vivo*. *J. Bacteriol.* **195,** 2880–2886 CrossRef Medline
29. DalCorso, G., Farinati, S., Maistri, S., and Furini, A. (2008) How plants cope with cadmium: staking all on metabolism and gene expression. *J. Integr. Plant Biol.* **50,** 1268–1280 CrossRef Medline
30. Verbruggen, N., Hermans, C., and Schat, H. (2009) Mechanisms to cope with arsenic or cadmium excess in plants. *Curr. Opin. Plant Biol.* **12,** 364–372 CrossRef Medline
31. Zhai, Z., Gayomba, S. R., Jung, H. I., Vimalakumari, N. K., Piñeros, M., Craft, E., Rutzke, M. A., Danku, J., Lahner, B., Punshon, T., Guerinot, M. L., Salt, D. E., Kochian, L. V., and Vatamaniuk, O. K. (2014) OPT3 is a phloem-specific iron transporter that is essential for systemic iron signaling and redistribution of iron and cadmium in *Arabidopsis*. *Plant Cell* **26,** 2249–2264 Medline
32. De Michele, R., Vurro, E., Rigo, C., Costa, A., Elviri, L., Di Valentin, M., Careri, M., Zottini, M., Sanità di Toppi, L., and Lo Schiavo, F. (2009) Nitric oxide is involved in cadmium-induced programmed cell death in *Arabidopsis* suspension cultures. *Plant Physiol.* **150,** 217–228 CrossRef Medline

33. Kulik, A., Anielska-Mazur, A., Bucholc, M., Koen, E., Szymanska, K., mieńko, A., Krzywińska, E., Wawer, I., McLoughlin, F., Ruszkowski, D., Figlerowicz, M., Testerink, C., Sklodowska, A., Wendehenne, D., and Dobrowolska, G. (2012) SNF1-related protein kinases type 2 are involved in plant responses to cadmium stress. *Plant Physiol.* **160,** 868–883 CrossRef Medline
34. Winter, D., Vinegar, B., Nahal, H., Ammar, R., Wilson, G. V., and Provart, N. J. (2007) An "Electronic Fluorescent Pictograph" browser for exploring and analyzing large-scale biological data sets. *PLoS ONE* **2,** e718 CrossRef Medline
35. Pierce, M. M., Raman, C. S., and Nall, B. T. (1999) Isothermal titration calorimetry of protein–protein interactions. *Methods* **19,** 213–221 CrossRef Medline
36. Abdullah, N., Padmanarayana, M., Marty, N. J., and Johnson, C. P. (2014) Quantitation of the calcium and membrane binding properties of the C2 domains of dysferlin. *Biophys. J.* **106,** 382–389 CrossRef Medline
37. Wang, A., Deems, R. A., and Dennis, E. A. (1997) Cloning, expression, and catalytic mechanism of murine lysophospholipase I. *J. Biol. Chem.* **272,** 12723–12729 CrossRef Medline
38. Wang, A., Loo, R., Chen, Z., and Dennis, E. A. (1997) Regiospecificity and catalytic triad of lysophospholipase I. *J. Biol. Chem.* **272,** 22030–22036 CrossRef Medline
39. Meier, R., Drepper, T., Svensson, V., Jaeger, K. E., and Baumann, U. (2007) A calcium-gated lid and a large β-roll sandwich are revealed by the crystal structure of extracellular lipase from *Serratia marcescens*. *J. Biol. Chem.* **282,** 31477–31483 CrossRef Medline
40. Gutiérrez-Fernández, J., Vaquero, M. E., Prieto, A., Barriuso, J., Martínez, M. J., and Hermoso, J. A. (2014) Crystal structures of *Ophiostoma piceae* sterol esterase: structural insights into activation mechanism and product release. *J. Struct. Biol.* **187,** 215–222 CrossRef Medline
41. Vijayaraj, P., Jashal, C. B., Vijayakumar, A., Rani, S. H., Venkata Rao, D. K., and Rajasekharan, R. (2012) A bifunctional enzyme that has both monoacylglycerol acyltransferase and acyl hydrolase activities. *Plant Physiol.* **160,** 667–683 CrossRef Medline
42. Lee, L. C., Lee, Y. L., Leu, R. J., and Shaw, J. F. (2006) Functional role of catalytic triad and oxyanion hole-forming residues on enzyme activity of *Escherichia coli* thioesterase I/protease I/phospholipase L1. *Biochem. J.* **397,** 69–76 CrossRef Medline
43. Karlsson, M., Contreras, J. A., Hellman, U., Tornqvist, H., and Holm, C. (1997) cDNA cloning, tissue distribution, and identification of the catalytic triad of monoglyceride lipase: evolutionary relationship to esterases, lysophospholipases, and haloperoxidases. *J. Biol. Chem.* **272,** 27218–27223 CrossRef Medline
44. Hariharan, P., Balasubramaniam, D., Peterkofsky, A., Kaback, H. R., and Guan, L. (2015) Thermodynamic mechanism for inhibition of lactose permease by the phosphotransferase protein IIA^{Glc}. *Proc. Natl. Acad. Sci. U.S.A.* **112,** 2407–2412 CrossRef Medline
45. Ma, Y., Szostkiewicz, I., Korte, A., Moes, D., Yang, Y., Christmann, A., and Grill, E. (2009) Regulators of PP2C phosphatase activity function as abscisic acid sensors. *Science* **324,** 1064–1068 Medline
46. Santiago, J., Rodrigues, A., Saez, A., Rubio, S., Antoni, R., Dupeux, F., Park, S. Y., Márquez, J. A., Cutler, S. R., and Rodriguez, P. L. (2009) Modulation of drought resistance by the abscisic acid receptor PYL5 through inhibition of clade A PP2Cs. *Plant J.* **60,** 575–588 CrossRef Medline
47. Lung, S. C., Liao, P., Yeung, E. C., Hsiao, A. S., Xue, Y., and Chye, M. L. (2017) Acyl-CoA-binding protein ACBP1 modulates sterol synthesis during embryogenesis. *Plant Physiol.* **174,** 1420–1435 CrossRef Medline
48. Lung, S. C., Liao, P., Yeung, E. C., Hsiao, A. S., Xue, Y., and Chye, M. L. (2018) *Arabidopsis* ACYL-COA–BINDING PROTEIN1 interacts with STEROL C4–METHYL OXIDASE1–2 to modulate gene expression of homeodomain-leucine zipper IV transcription factors. *New Phytol.* **218,** 183–200 CrossRef Medline
49. Taskinen, J. P., van Aalten, D. M., Knudsen, J., and Wierenga, R. K. (2007) High resolution crystal structures of unliganded and liganded human liver ACBP reveal a new mode of binding for the acyl-CoA ligand. *Proteins* **66,** 229–238 Medline
50. Li, M., Bahn, S. C., Guo, L., Musgrave, W., Berg, H., Welti, R., and Wang, X. (2011) Patatin-related phospholipase pPLAIIIβ-induced changes in lipid metabolism alter cellulose content and cell elongation in *Arabidopsis*. *Plant Cell* **23,** 1107–1123 Medline
51. Ho, S. N., Hunt, H. D., Horton, R. M., Pullen, J. K., and Pease, L. R. (1989) Site-directed mutagenesis by overlap extension using the polymerase chain reaction. *Gene* **77,** 51–59 CrossRef Medline
52. Fong, Y. H., Wong, H. C., Chuck, C. P., Chen, Y. W., Sun, H., and Wong, K. B. (2011) Assembly of preactivation complex for urease maturation in *Helicobacter pylori*: crystal structure of UreF–UreH protein complex. *J. Biol. Chem.* **286,** 43241–43249 CrossRef Medline
53. Hong, Y., Wang, T. W., Hudak, K. A., Schade, F., Froese, C. D., and Thompson, J. E. (2000) An ethylene-induced cDNA encoding a lipase expressed at the onset of senescence. *Proc. Natl. Acad. Sci. U.S.A.* **97,** 8717–8722 CrossRef Medline
54. Ishiguro, S., Kawai-Oda, A., Ueda, J., Nishida, I., and Okada, K. (2001) The *DEFECTIVE IN ANTHER DEHISCENCE1* gene encodes a novel phospholipase A1 catalyzing the initial step of jasmonic acid biosynthesis, which synchronizes pollen maturation, anther dehiscence, and flower opening in *Arabidopsis*. *Plant Cell* **13,** 2191–2209 Medline
55. Hsu, K. H., Wang, S. Y., Chu, F. H., and Shaw, J. F. (2010) Characterization and heterologous expression of a novel lysophospholipase gene from *Antrodia cinnamomea*. *J. Appl. Microbiol.* **108,** 1712–1722 CrossRef Medline
56. Suzuki, T., Shibuya, Y., Sato, T., Nishizawa, S., Sato, I., and Yamaguchi, A. (2016) Thermodynamics of complexation between thiourea-based receptor and acetate in water/acetonitrile mixture. *Anal. Sci.* **32,** 741–744 CrossRef Medline
57. Fiser, A., and Šali, A. (2003) Modeller: generation and refinement of homology-based protein structure models. *Methods Enzymol.* **374,** 461–491 CrossRef Medline
58. Sali, A., Potterton, L., Yuan, F., van Vlijmen, H., and Karplus, M. (1995) Evaluation of comparative protein modeling by MODELLER. *Proteins* **23,** 318–326 CrossRef Medline
59. Sánchez, R., and Šali, A. (2000) Comparative protein structure modeling: introduction and practical examples with modeller. *Methods Mol. Biol.* **143,** 97–129 Medline
60. Morris, G. M., Huey, R., Lindstrom, W., Sanner, M. F., Belew, R. K., Goodsell, D. S., and Olson, A. J. (2009) AutoDock4 and AutoDockTools4: automated docking with selective receptor flexibility. *J. Comput. Chem.* **30,** 2785–2791 CrossRef Medline
61. Tzeng, S. R., and Kalodimos, C. G. (2009) Dynamic activation of an allosteric regulatory protein. *Nature* **462,** 368–372 CrossRef Medline
62. Tzeng, S. R., and Kalodimos, C. G. (2012) Protein activity regulation by conformational entropy. *Nature* **488,** 236–240 Medline
63. Waterhouse, A. M., Procter, J. B., Martin, D. M., Clamp, M., and Barton, G. J. (2009) Jalview Version 2–a multiple sequence alignment editor and analysis workbench. Bioinformatics 25, 1189–1191 CrossRef Medline